Carbohydrate Polymers 294 (2022) 119777

Contents lists available at ScienceDirect

Carbohydrate Polymers

journal homepage: www.elsevier.com/locate/carbpol

Aspidopterys obcordata vine inulin fructan affects urolithiasis by modifying calcium oxalate crystallization

Peng Sun [a,c], Shang-Gao Liao [b], Rao-Qiong Yang [a,c,e], Chuan-Li Lu [d], Kai-Long Ji [a], Dong-Hua Cao [a,f], Hua-Bin Hu [a,c], Jian-Mei Lu [a,c], Xing-Zhen Song [a], Min Wu [a,c], Hui-Zhen Jia [a,c], Chun-Fen Xiao [a], Zhi-Wei Ma [a], You-Kai Xu [a,*]

[a] *Key Laboratory of Tropical Plant Resources and Sustainable Use, Xishuangbanna Tropical Botanical Garden, Chinese Academy of Sciences, Menglun, Mengla, Yunnan 666303, China*
[b] *School of Pharmacy, State Key Laboratory of Functions and Applications of Medicinal Plants, Guizhou Medical University, Guiyang, Guizhou 550004, China*
[c] *University of Chinese Academy of Sciences, Beijing 100049, China*
[d] *Institute of Nanfan & Seed Industry, Guangdong Academy of Sciences, Guangzhou, Guangdong 510316, China*
[e] *Key Laboratory of Tropical Forest Ecology, Xishuangbanna Tropical Botanical Garden, Chinese Academy of Sciences, Menglun, Mengla, Yunnan 666303, China*
[f] *The Affiliated Changsha Central Hospital, Hengyang Medical School, University of South China, Changsha 410004, China*

ARTICLE INFO

Keywords:
Calcium oxalate
Fructan
Aspidopterys obcordate
Anti-urolithiasis
Fruit fly

ABSTRACT

Aspidopterys obcordata vine is a Chinese Dai ethnic herb used to treat urolithiasis. However, the material basis and underlying mechanisms remain undefined. In this study, a 2.3 kD inulin-like *A. obcordata* fructan (AOFOS) was isolated by size exclusion column chromatography and characterized by ultrahigh-performance liquid chromatography-ion trap-time of flight mass spectrometry (UPLC-IT-TOF-MS), nuclear magnetic resonance (NMR) spectroscopy, gas chromatography mass spectrometry (GC–MS) and high-performance gel permeation chromatography (HGPC). In addition, AOFOS showed unique anti-urolithiasis activity in *Drosophila* kidney stone models. Mechanism study indicated that AOFOS reduced the size of calcium oxalate crystals by inhibiting the formation of large size crystals and the generation rate of calcium oxalate crystals as well as the crystal form conversion from calcium oxalate monohydrate (COM) to calcium oxalate dihydrate (COD).

1. Introduction

Urolithiasis (e.g., renal calculus) is an anomalous process of biomineralization (Daudon et al., 2014) with multimorbidity and easy recurrence (Sorokin et al., 2017). Its recurrence rate is 50 % within 10 years and >75 % within 15 years of the first stone episode in developing countries (Penniston et al., 2011). Excess consumption of oxalate, seasonal high temperature (Chen et al., 2008), and low fluid intake (Lotan et al., 2013) were reported to be related to its formation. Meanwhile, disease factors such as obesity (Taylor et al., 2010) and diabetes may directly increase the glomerular filtration rate and cause the occurrence of stones. Urolithiasis is generally treated with surgery (Türk et al., 2016). However, its high recurrence rate and high cost of treatment makes drug treatment particularly indispensable. Drug therapy is generally aimed at preventing the formation of small stones (e.g., use of stone inhibitors), speeding up the diuretic process after the discharge of graves (with diuretics) or reducing inflammation and complications (e.g., use of spasmodic and analgesic drugs or anti-inflammatory drugs) (Spernat & Kourambas, 2011).

The mechanism of urolithiasis is not fully understood; however, calcium oxalate occurs in 70 % to 80 % of urolithiasis cases (Ansari et al., 2005) and has become the focus of lithiasis research. It has been proven that initialization of lithiasis begins with the generation of crystal nuclei and their adhesion to the injury site of epithelial cells (Gan et al., 2016; Semangoen et al., 2008), while continuous growth of crystals (Asselman et al., 2005; Li et al., 2017) will result in crystals of excessive size, which will ultimately lead to urinary tract obstruction and lesions (Aggarwal et al., 2013). Calcium oxalate monohydrate (COM) and calcium oxalate dihydrate (COD) have been proved to have different physical properties and cytotoxicity (Sun et al., 2015). Reduction or clearance of calcium oxalate crystals has been deemed a therapeutic strategy for urolithiasis treatment (Grohe et al., 2007; Trinchieri et al., 2005).

Herbal medicine has been used in the treatment of urolithiasis worldwide (Khan et al., 2021). In the Dai minority region of China, the

* Corresponding author.
E-mail address: xyk@xtbg.ac.cn (Y.-K. Xu).

https://doi.org/10.1016/j.carbpol.2022.119777
Received 15 February 2022; Received in revised form 30 May 2022; Accepted 21 June 2022
Available online 25 June 2022

perennial woody vine of *Aspidopterys obcordata* (Hei Gai Guan) has been used a fork medicine for treating urinary tract infection, cystitis and urinary tract stones (Lin et al., 2003) and also treated as a drink for preventing kidney stones. More than 50 compounds including steroids, glycosides, terpenoids, phenols, phenylpropanin, glycosides and lignin have been identified and reported to be present in the plant (Hu et al., 2018; Sun et al., 2020), and pharmacological investigations showed that the extract of *A. obcordata* could protect against oxalate-induced damage in renal tubular epithelial cells (HK-2) and effectively inhibit the formation of calcium oxalate crystals in the rat kidney (Li et al., 2016; Song et al., 2015). The steroidal saponin obcordata A obtained from this plant prevented against kidney stones through the NOX4/ROS/P38 MAPK oxidative stress pathway (Li et al., 2019).

Previous studies suggested that the secondary metabolites of *A. obcordata* showing capacity of reducing inflammation and oxidative stress were responsible for its therapeutic effect on urolithiasis (Aggarwal et al., 2013; Li et al., 2019; Sun et al., 2020). However, the discovery that the water-soluble fraction of the water extract could significantly reduce the crystal size of calcium oxalate in a rat model indicated that the polysaccharides or proteins present in the fraction could not be excluded as active principles for calcium oxalate crystal reduction. Since *Porphyra yezoensis* polysaccharides could inhibit the adhesion and endocytosis of crystals (Sun et al., 2021; Zhang, Hu, et al., 2020; Zhang, Sun, et al., 2020), degraded soybean polysaccharides could inhibit the crystallization of calcium oxalate (Yao et al., 2012), and carboxylate-modified inulin biopolymers could direct calcium oxalate crystallization from calcium oxalate monohydrate (COM) to calcium oxalate dihydrate (COD) (Akin et al., 2008), it is possible that the polysaccharides in *Aspidopterys obcordata* could also possess a similar effect.

Thus, in this study, an inulin-like polysaccharide purified from the aqueous extract of *Aspidopterys obcordata* (AOFOS) was evaluated for its inhibitory activity against calcium oxalate crystallization in vitro, in cells and in fruit fly models. The isolation and biological evaluation of AOFOS were reported.

2. Materials and methods

2.1. Materials and apparatus

A. obcordata was collected from Xishuangbanna Tropical Botanical Garden (XTBG), Chinese Academy of Science (CAS), Mengla County, Yunnan Province, People's Republic of China in September 2016, and was identified by one of the authors (Chun-Fen Xiao). A voucher specimen (No. HITBC_094469) has been deposited in the herbarium of XTBG.

Calcium chloride, oxalate dihydrate, and all chemicals were of analytical purity and were purchased from Damao Chemical Reagent Factory (Damao, China). All solvents used for HPLC were of spectral grade (Fisher Scientific, USA). Toyopearl HW-40 F (TOSOH, Japan) and Sephadex LH-20 gel (40–70 μm, Amersham Pharmacia Biotech AB, Sweden) were used for column chromatography. DMEM and fetal bovine serum (FBS) were purchased from HyClone Biochemical Products Co. Ltd. (HyClone, USA). MTS Cell Proliferation Colorimetric Assay Kit (Biovision, USA). Deionized water was obtained from the Millipore-Q system (Millipore, USA), and the resistance was 18.2 MΩ.

2.2. Extraction and purification of polysaccharides

The dried vine of *A. obcordata* (100 g) was grinded and sieved powder (100 mesh). The obtained powder was extracted with boiling water for three times (each for 30 min). The combined solution was concentrated under reduced pressure to remove *ca* 2/3 of water to give a water extract solution, and then methanol was added to the aqueous solution until a methanol concentration of 80 % was reached. The solution was kept at 4 °C for 24 h before being subjected to centrifugation (2000 rpm/min, 5 min, 3 times). Removal of the supernatant gave the crude polysaccharide (2.18 g) by rotary evaporators.

Purification of the crude polysaccharide on a Sephadex LH-20 column eluted with water gave a colorless fraction enriched in polysaccharides, further purification of which on an HW-40 column (26 mm × 50 cm) (Li et al., 2021) eluted with distilled water (3.0 mL/min, 10 mL/tube) and monitored by the Abbe refractometer method yielded AOFOS (20 mg) (Fig. S1). UV analysis at 260 and 280 nm and ferric chloride test is used to detect the presence of protein and tannin.

2.3. Characterization of A. obcordata fructan (AOFOS)

2.3.1. Molecular weight of AOFOS

The molecular weight of AOFOS was estimated by gel permeation column chromatography on an Ultrahydrogel™ linear column (7.8 × 300 mm) at 40 °C eluted with a solution of $NaNO_3$ (0.1 mol/L) at a flow rate of 1.0 mL/min. The injected volume was 50 μL and the concentration of the biopolymer was 1 mg/mL. Pullulan samples (Shodex Standard P-82, Phenomenex) were used as standards for the construction of the calibration curve.

2.3.2. NMR analysis of AOFOS

The dried samples of AOFOS (10 mg) were dissolved in 0.3 mL of D_2O in a nuclear magnetic tube. ^1H and ^{13}C NMR spectra were recorded on a Bruker Avance spectrometer conducting at 500 and 125 MHz, respectively. 2D NMR spectra [heteronuclear single-quantum coherence (HSQC), shift correlation spectroscopy (COSY) and heteronuclear multiple-bond correlation (HMBC)] were obtained using standard Bruker procedures (Sun et al., 2020).

2.3.3. Monosaccharide composition analysis of AOFOS

The monosaccharide composition of AOFOS was determined using the 1-phenyl-3-methyl-5-pyrazolone (PMP) pre-column derivatization method (Zhang et al., 2021). Liquid chromatography mass spectrometry (LC-MS) and gas chromatography–mass spectrometry (GC–MS) were used to analyze AOFOS according to the literature method (De Oliveira et al., 2011; Dominique et al., 2008; Li et al., 2018). The detailed procedures are appended in the Supplementary data.

2.4. Effect of AOFOS on Drosophila Malpighian tubule model

2.4.1. Culture of fruit fly

Drosophila melanogaster flies were obtained from the Kunming Institute of Zoology, Chinese Academy of Sciences. *D. melanogaster* flies were maintained at 25 °C and 50 % humidity with 12-h light-dark cycles in a medium containing 1 % (wt/vol) agar, 2 % (wt/vol) yeast, 6 % (wt/vol) glucose, 8 % (vol/vol) soluble starch, and 0.08 % (wt /vol) benzoic acid (Chen et al., 2011). All adult *D. melanogaster* experiments were performed in plastic vials with Vent Cap Sterile.

2.4.2. Calcium oxalate model

Female Drosophila were starved for 12 h and divided into two groups (model group and AOFOS group) with 20 flies in each group. Each group was given 0.1 % (wt/vol) oxalic acid to reproduce a calcium oxalate model (Ali et al., 2018), and was given AOFOS (1 mg/mL, for AOFOS group) or vehicle (for model group). Three flies were removed every 24 h and killed with carbon dioxide. The Malpighian tubes were then dissected and observed under a polarizing microscope.

2.5. Crystal growth inhibition assay

2.5.1. Crystal preparation

Stock solutions of oxalic acid and calcium chloride (2, 5 and 10 mM) and AOFOS (1, 0.5, 0.25 and 0.125 mg/mL) were prepared with water. Calcium chloride solution was placed into EP tubes or 96-well plates, and 3 replicates were performed in each group. The EP tube or 96-well plate was preheated on a microplate heating oscillator (T75 °C, medium

speed oscillation) for 2 min. Equal volumes of AOFOS and oxalic acid solution were added to each group in sequence. Observations and measurements were made according to experimental procedure reported (Sun et al., 2015).

2.5.2. Morphological analysis

Crystal (5 mM) suspensions collected under the induction of AOFOS at different concentrations were dispersed on a 10 mm × 10 mm glass slide and dried at 50 °C temperature. The samples were firstly examined under a polarization microscope, and then observed at 6000-fold magnification by scanning electron microscopy (SEM) operated at 10 kV after being sputtered with a layer of carbon using a sputter coater.

2.5.3. FT-IR spectrum

Crystal (10 mM) suspensions were collected under the induction of 100 μL of AOFOS solutions at different concentrations, dried at 50 °C and then mixed with KBr. After grinded and pressed into KBr pellets, scanning was performed between 4000 cm^{-1} and 400 cm^{-1}.

2.5.4. Formation rate of crystal

First, 98 μL of 2 mM calcium chloride mixed with different concentrations of AOFOS was added to the 96-well plate, and then 2 μL of 100 mM oxalic acid was added. The supernatant was removed every 4 min, and the density was detected at absorbance 630 nm after 20 min by a microplate reader.

2.6. Cell culture

NRK-52E (normal rat epithelial cells) was supplied by Central South University. Cells were maintained as continuously growing monolayers in 25 cm^2 culture flasks (Gibco company, USA) in DMEM supplemented with 10 % fetal bovine serum (FBS) and 1 % streptomycin antibiotics at 37 °C in a 5 % CO_2 air atmosphere incubator. When the cells reached an 80–90 % fusion monolayer, trypsin was digested and gently mixed into the cells to form a single-cell suspension for subsequent cell experiments. A cell suspension with a concentration of 1×10^5 cells/mL was seeded in each well of a 96-well plate and cultured in medium for 24 h (Yasui et al., 2001).

(1) Toxicity of AOFOS to NRK-52E cells: (A) Normal control group: serum-free medium; (B) AOFOS group: serum-free medium containing different concentrations of AOFOS.
(2) Toxicity of oxalic acid at different concentrations of AOFOS (Peng et al., 2021): (A) Normal control group: serum-free medium; (B) Injury control group: serum-free medium containing 2 mM oxalic acid. (C) Oxalic acid + AOFOS group: serum-free medium containing different concentrations of AOFOS + 2 mM oxalic acid.
(3) Toxicity of crystals precipitated and supernatant induced by oxalic acid at different concentrations of AOFOS. 2 mM oxalic acid was added to serum-free medium with different concentrations of AOFOS to induce crystals and precipitate for 3 h. After centrifugation, the cells were cultured with supernatant and precipitated.

After treatment for 24 h, 20 μL MTS was added to each well and incubated for 2 h at 37 °C. Absorbance was measured by using a microplate reader instrument at 492 nm, and cell viability was thus calculated.

2.7. Data analysis

The results are expressed as the mean ± standard deviation (SD). The data were analyzed via one-way analysis of variance (ANOVA) or Student's *t*-tests. Values of $P < 0.05$ were considered statistically significant. All computations for this article were performed using R (R Core Team, 2020).

3. Results

3.1. AOFOS was identified as an inulin-type fructan

Identification of the purity. The inulin-like polysaccharide solution does not turn green with the addition of ferric chloride, suggesting that it does not contain phenolic acids. Ultraviolet absorptions at 260 and 280 nm were not observed, indicating the absence of proteins or peptides.

The MS of AOFOS (Fig. S3) showed the obvious molecular ion peaks at 364.9470, 527.4487, 670.9086, 841.9006, 1003.901, 1165.8759, 1328.3656, 1490.3215, 1652.3154, 1814.7648, 1976.1688 and 2138.5913, where a mass difference of 162 corresponding to successive loses of fructose between two neighboring ions was observed and the maximum abundance at *m/z* 1490.3215 was assumed to be $[GF_8 + NH_4]^+$ (De Oliveira et al., 2011). Although the MS data obtained in the LC-IT-TOF system only showed *m/z* values lower than 5000 and only *m/z* values lower than 2200 were detected in the spectrum, the current LC-IT-TOF-MS data provided information for its constitutional feature as an inulin-type fructan.

Monosaccharide composition analysis results of AOFOS were shown in Figs. S6 and S7. Briefly, a minor peek corresponding to the PMP-derivative of glucose was observed in the HPLC-PDA analysis of its hydrolysate derivative. Intense fructose and weak glucose derivatives were observed in the GC–MS chromatogram of its hydrolysate derivative (Fig. S7) and the area ratio of fructose to glucose derivatives was determined to be *ca* 13:1 by their extracted ion chromatograms (EICs) (Table S2). The molecular ratio of fructose to glucose in AOFOS was therefore determined to be 13:1.

The ^1H NMR and ^{13}C NMR spectra of AOFOS displayed the typical characteristics of polysaccharides (Mensink et al., 2015; Roberfroid, 2005; Zhang, Hu, et al., 2020). One minor peak at 5.34 ppm, two intense peaks centered at 4.16 and 4.01 ppm, together with a cluster of signals between 3.62 and 3.83 ppm were observed in the ^1H NMR spectrum. The ^{13}C NMR spectra of AOFOS displayed the presence of six carbon signals, which were further classified as two methylenes (60.8 and 62.1 ppm), three methines (74.2, 76.9, and 81.0 ppm) and one quaternary carbon (103.2 ppm) by the DEPT experiment (Fig. 1a, b).

The protons and carbons of the preponderant residues were unequivocally assigned by 2D NMR correlation analysis (Table 1). The signal at δ_H 5.34/δ_C 92.5 ppm correlated to each other in the anomeric region in the HSQC spectrum (Fig. 1c) indicated the presence of an α-D-glucopyranosyl residue (Zhang, Hu, et al., 2020). The key correlations of the ^1H-^1H COSY and HMBC spectra of AOFOS (Fig. 1d, e) showed that the polysaccharide was composed of fructose with a terminal α-D-glucopyranosyl residue. The HMBC correlation from the anomeric signal of the glucosyl residue to Fruf-C-2 suggested that the terminal α-D-glucopyranosyl was located at C-2 position of a fructosyl residue. The strong HMBC correlations from H-3 to C-1, C-2, and C-4 as well as from H-4 to C-3, C-5, and C-6 were consistent with the presence of a fructosyl residue. Fructans are mainly composed of inulin (2,1-linked-D-Fruf) or levans (2,6-linked-D-Fruf) (Han & Clarke, 1990). The similar ^{13}C NMR data of the fructosyl residues between AOFOS and LCPS (Zhang, Hu, et al., 2020), along with the HMBC correlation between C-2 and H-1 of the fructosyl residue proved the existence of a 2,1-linkage between fructosyls, and then, the concomitant correlation peaks were located at between C-2 of a fructosyl residue and H-1 of the fructosyl residue. While the ROESY correlation (Fig. S5) between Fruf-H-1 and Fruf-H-3 indicated a β-configuration for the fructosyl.

A proton integral ratio (*ca* 26:1, Fig. S4) of H3-Fruf and H4-Fruf to H1-Glcp suggest a degree of polymerization (DP) of approximately 13. This conclusion can also be verified from the GPC information shown in Fig. S2. The molecular weights (Mp) of AOFOS were estimated to be approximately 2.3 kD (Li et al., 2018). Taken together, AOFOS was therefore determined to be α-D-Glcp-(1 → 2) -[β-D-Fruf-(2 → 1)- β-D-Fruf] $_{12}$-(2 → 1)- β-D-Fruf (Fig. 1f), a typical inulin-type fructan.

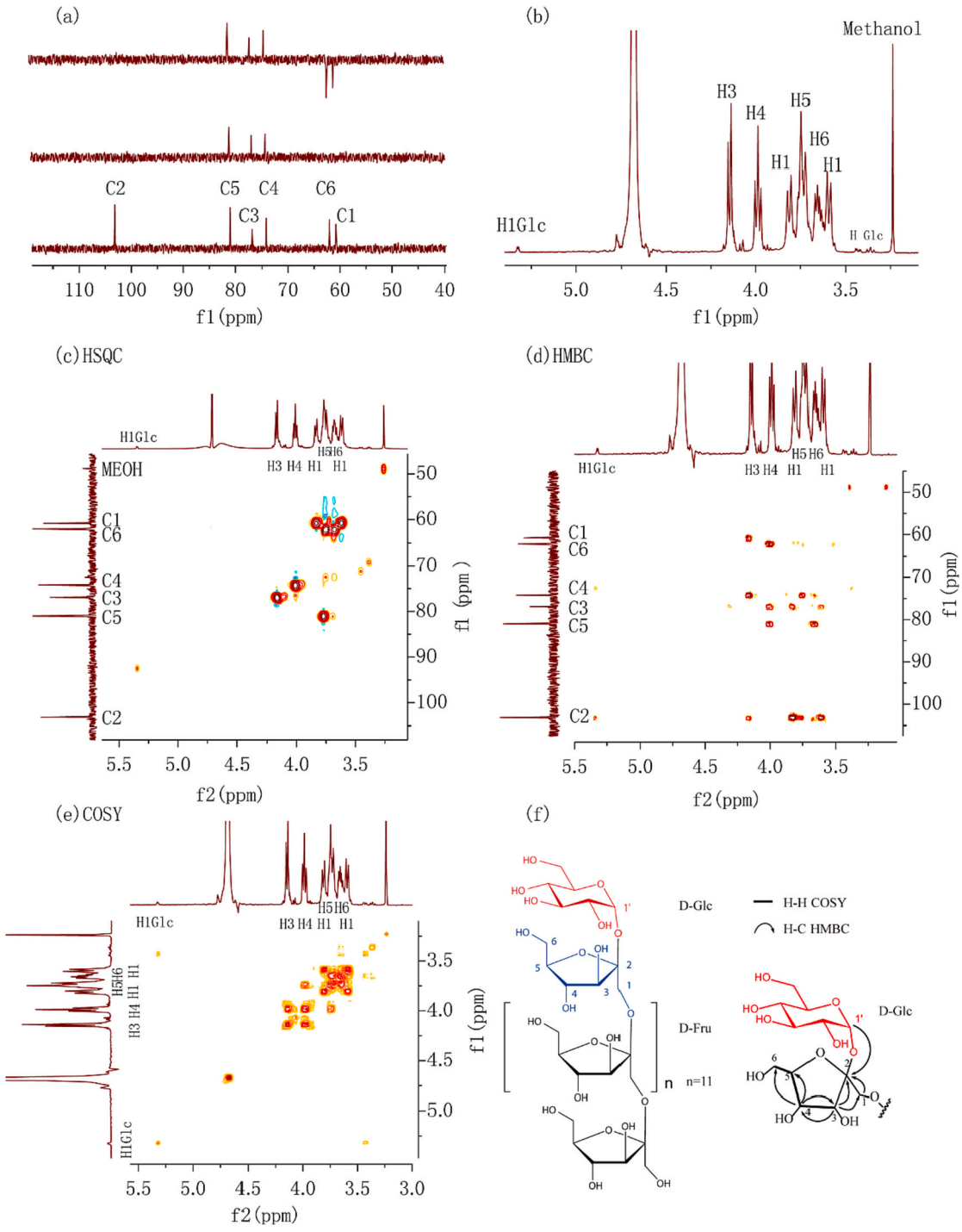

Fig. 1. Structure elucidation of AOFOS. (a) ^{13}C NMR (125 MHz, D_2O). (b) ^{1}H NMR (500 MHz, D_2O). (c) HSQC spectrum (600 MHz, D_2O). (d) HMBC spectrum. (e) ^{1}H-^{1}H COSY spectrum. (f) Structure and key correlation of AOFOS.

3.2. Effect of AOFOS on crystallization induced by oxalic acid in Drosophila

The model of oxalate-induced calcium oxalate crystals in Malpighian tubules in Drosophila has been widely used to simulate urolithiasis in vivo (Chen et al., 2011). The result of AOFOS on the formation of calcium oxalate crystals in Malpighian tubules observed by polarizing microscopy showed that AOFOS had no effect on the total crystal area; however, the crystal size in AOFOS group was obviously smaller than that in the model group at high magnification (20×). Meanwhile, the crystal morphology tended to be round without sharp edges and corners in the AOFOS group, but was sharp and irregular in the model group (Fig. 2a, b).

To clearly demonstrate the influence of AOFOS on the size of calcium oxalate crystals, six pairs of Malpighian tubules from three flies in each group were dissected and analyzed by ImageJ software. The total area of crystals in Malpighian tubules was measured in the whole field of view (700 μm × 100 μm, 20× magnification). The quantified data of four grades (1–4, 5–40, 41–400, and 401–1000 μm^2) showed that AOFOS could significantly inhibit the formation of larger crystals (> 200 μm^2) and induce small crystals (<10 μm^2) (Fig. 2c).

Table 1
Assignments of the ^{1}H and ^{13}C NMR spectra of AOFOS.

No. of C/H	^{1}H	^{13}C
β-D-Fruf-2,1		
1	3.62, 3.83	60.8
2	–	103.2
3	4.16	76.9
4	4.01	74.2
5	3.77	81.0
6	3.74, 3.68	62.1
α-D-Glcp		
1	5.34	92.5

Detailed data in supplementary data.

3.3. Inhibition of crystal growth and induction of COD formation

3.3.1. Effect on the shape of crystals

To study the interaction mechanism between AOFOS and calcium oxalate crystals, calcium oxalate crystals were created in vitro according to the literature (Sun et al., 2015). Scanning electron microscopy (SEM) results (Fig. 3) showed that large crystals and heterogeneous crystals were dominant in the untreated group, while tiny crystals were formed in AOFOS groups with different concentrations. The crystal size significantly ($p < 0.05$) decreased from 1.74 ± 0.56 to 0.68 ± 0.18 μm^2 (Fig. 3d) when the concentration of AOFOS increased from 0 to 333 μg/mL. Meanwhile, the crystals were changed from sharp hexagonal to round at 42 μg/mL and above, which suggested that calcium oxalate crystals were changed from COM to COD (Liu et al., 2020; Yao et al., 2012).

3.3.2. Effect on the characteristics of crystals

There were significant differences between COM and COD crystals in the FT-IR spectra (Sun et al., 2015). For COM crystals, there were multiple peaks at 3000–3600 cm^{-1}, while for COD crystals, only a single wide absorption peak at 3445 cm^{-1} was observed (Maurice-Estepa et al., 2000). FT-IR spectra of 10 mM COM crystals treated with different concentrations of AOFOS showed that transformation of COM to COD crystals could be induced by AOFOS in a concentration-dependent manner (Fig. 4).

3.3.3. Effect on the formation rate of crystals

The crystal formation process was observed. The crystal first formed small crystal nuclei in the solution, then gradually increased in volume and finally existed at the bottom of the container in the form of

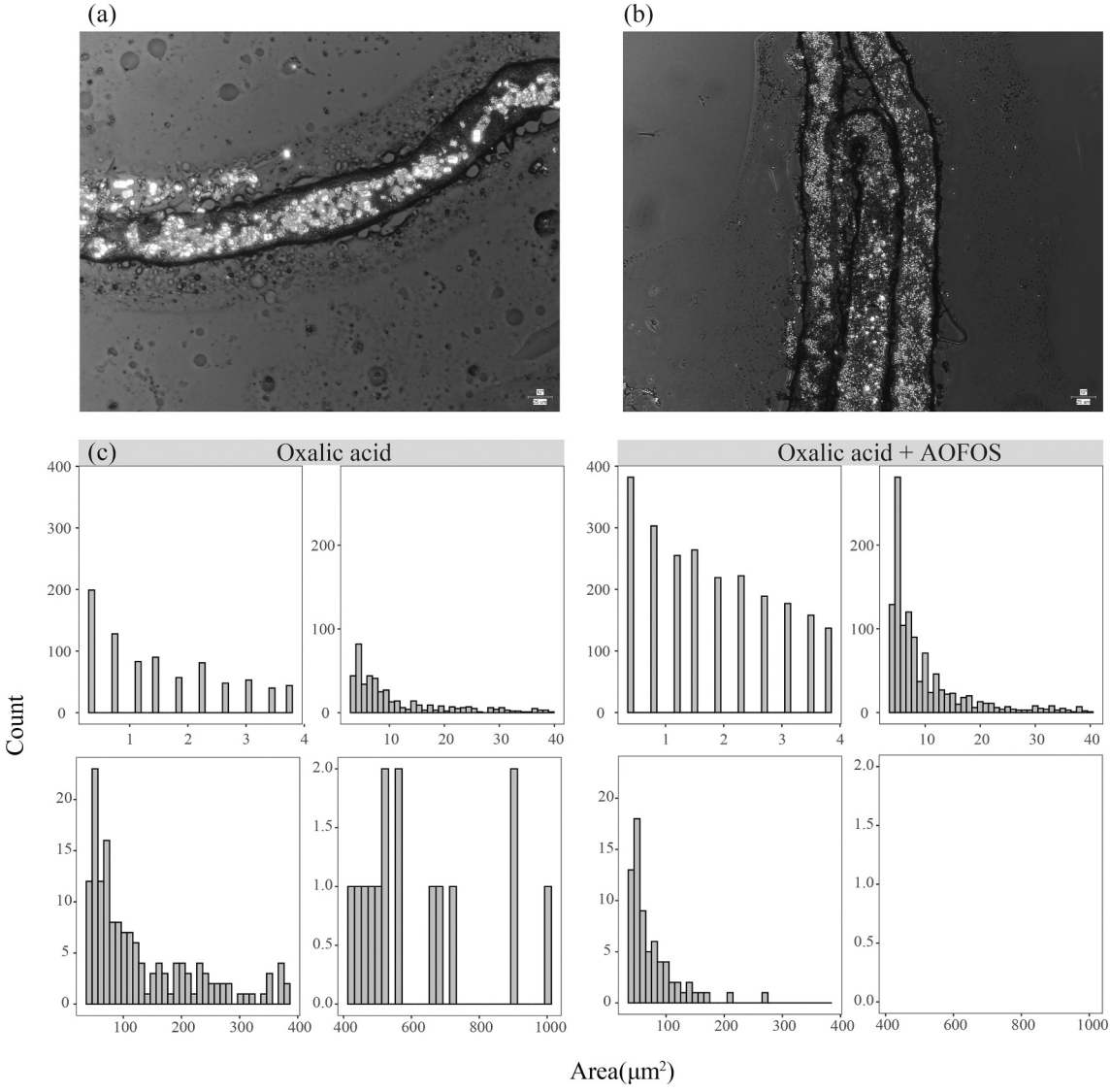

Fig. 2. Effect of OFOS on calcium oxalate crystal deposition in Malpighian tubules. (a) Polarized image of Malpighian tubules from the model group. (b) Polarized image of Malpighian tubules from AOFOS (1 mg/mL) group. (c) Area distribution of calcium oxalate crystals with different treatments in the Malpighian tubules.

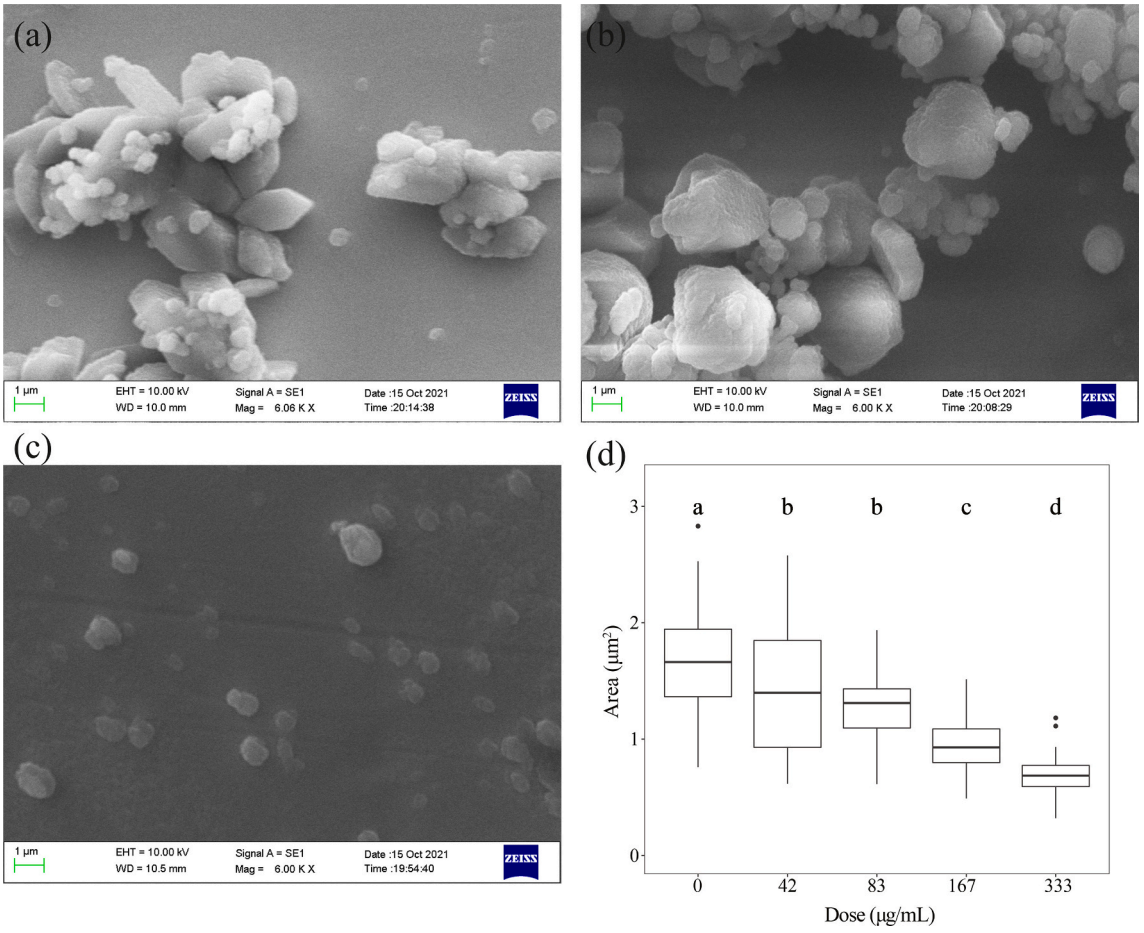

Fig. 3. Effect of AOFOS on calcium oxalate crystal size. (a–c) SEM images of calcium oxalate crystal formed in the presence of various concentrations of AOFOS: (a) blank control, (b) 42 μg/mL and (c) 333 μg/mL. (d) Area of distribution of calcium oxalate crystal induced by AOFOS. c(CaOxa) = 5 mM. Data were expressed as mean ± SD from experiments, different letters indicate significant differences (repeated ANOVA, $p < 0.05$).

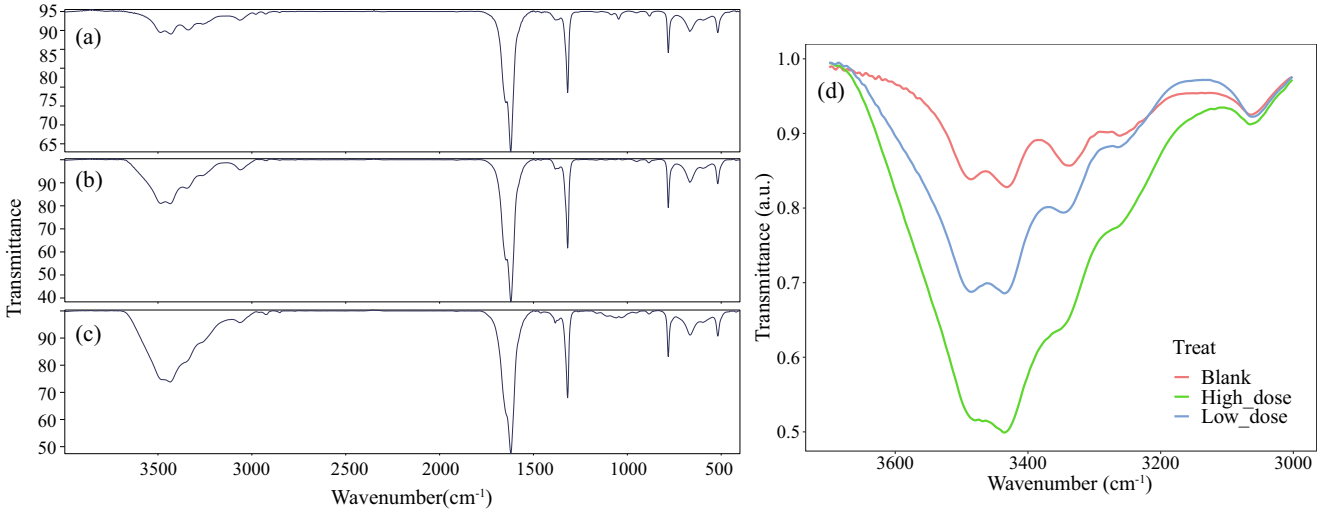

Fig. 4. AOFOS induced the conversion of COM to COD. (a–c) FT-IR spectrum of COM crystals induced by various concentrations AOFOS: (a) blank; (b) 83 μg/mL and (c) 333 μg/mL. c(CaOxa) = 10 mM. (d) Feature absorption wavelength (4000–3000 cm^{-1}) of COM crystals induced by various concentrations AOFOS: blank (red); 83 μg/mL AOFOS (blue) and 333 μg/mL AOFOS (green). c(CaOxa) = 10 mM.

precipitation. As indicated in Fig. 5a, a hexagonal and sharp shape was observed for crystals of the blank control and positive control (citric acid) groups; however, a diamond shape was formed for the AOFOS group at 4 min. Larger crystals continued to be formed in the blank control and positive control (citric acid) groups, while only small crystals were formed in the AOFOS group within 12–20 min. A concentration-dependent inhibitory effect on the crystal formation was also observed in crystal density measurement at 630 nm within 20 min

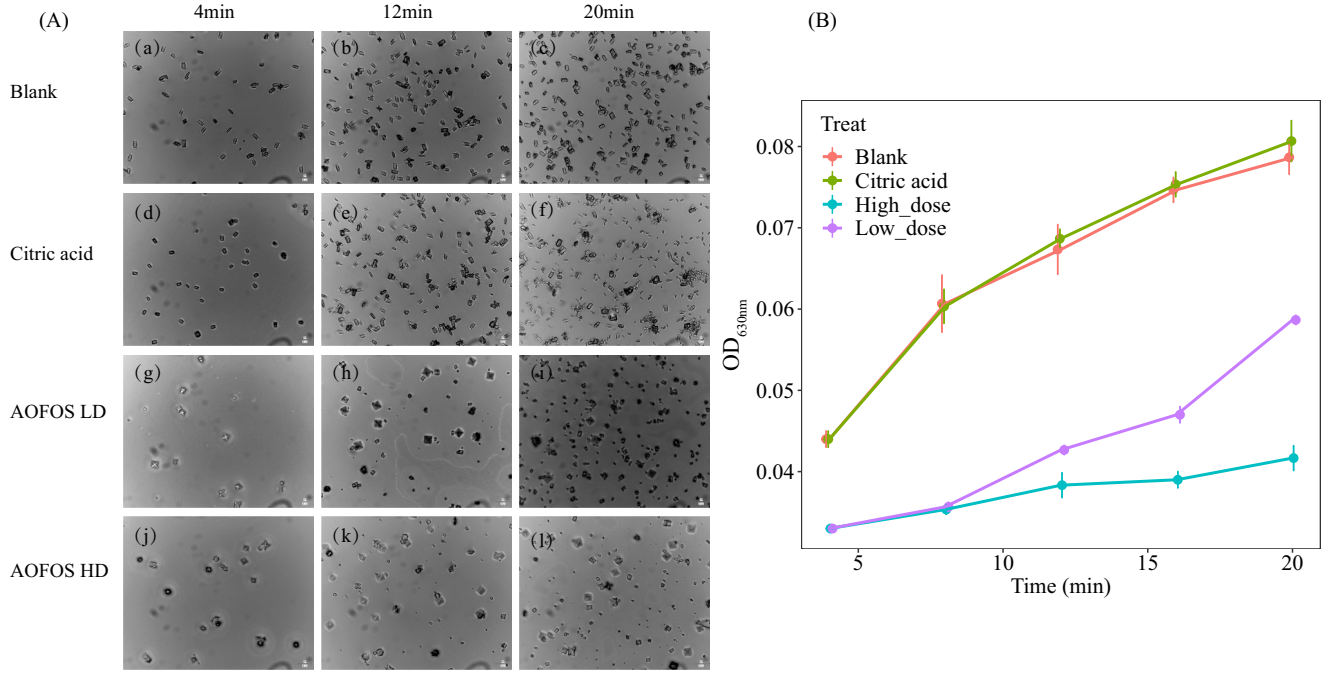

Fig. 5. AOFOS inhibited the formation rate of calcium oxalate crystals. (A) Polarizing microscope images of calcium oxalate crystal formed of different treatments at 4 min, 12 min and 20 min: (Blank) PBS; (Citric acid) Citric acid 200 μg/ml; (AOFOS LD) AOFOS 100 μg/ml and (AOFOS HD) AOFOS 200 μg/mL. c(CaOxa) = 2 mM. (B) Density of calcium oxalate crystal induced by Citric acid + OFOS: (orange)PBS; (green) citric acid 200 μg/mL; (purple) OFOS 100 μg/mL and (blue) OFOS 200 μg/mL. c(CaOxa) = 2 mM.

(Fig. 5b).

3.4. Effects of AOFOS on cells

3.4.1. Cytotoxicity of AOFOS

Cytotoxic activity of AOFOS against normal rat epithelial cells NRK-52E cells at 25, 50, 100 and 200 μg/mL (Fig. 6e) showed that AOFOS had no significant cytotoxicity, which indicated that AOFOS were safe at all concentrations below 200 μg/mL.

3.4.2. Effects of AOFOS on oxalic acid-induced cellular injury

Oxalate ions and calcium oxalate crystals play an important role in the process of occurrence and development of urolithiasis. The cytotoxicity of oxalic acid (2 mM) was reported (Song et al., 2015; Peng

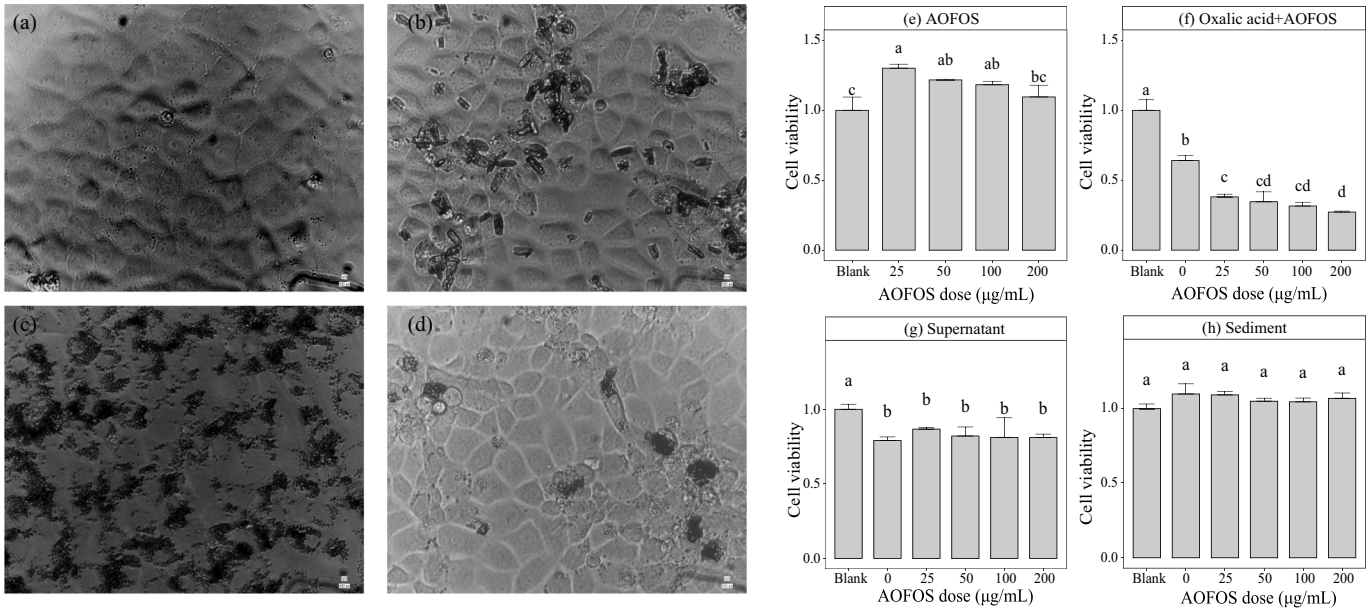

Fig. 6. Effect of AOFOS on NRK-52E. (a–d) Cell morphology: (a) Normal medium; (b) Medium with 2 mM oxalic acid; (c) Medium with 2 mM oxalic acid + 200 μg/mL AOFOS; (d) Supernatant medium induced by 2 mM oxalic acid 3 h. (e–h) Cell viability. (e) Toxicity of AOFOS to NRK-52E cells; (f) Cytotoxicity of 2 mM oxalic acid in the presence of different drugs; (g) Cytotoxicity culture medium supernatant induced 3 h by 2 mM oxalic acid in the presence of various concentrations AOFOS. (h) Cytotoxicity of culture medium sediment induced 3 h by 2 mM oxalic acid in the presence of various concentrations AOFOS. Data were expressed as mean ± SD from three independent experiments, compared with Blank group, different letters indicate significant differences between the cell viability (repeated ANOVA, $p < 0.05$).

et al., 2021). To verify whether AOFOS can inhibit the damage of oxalic acid on cells, the following experiments were carried out. Coincubation of NRK-52E cells without or with different concentrations of AOFOS and oxalic acid (2 mM) showed that oxalic acid itself significantly reduced cell viability, and increasing concentration of AOFOS increased the cytotoxicity in a concentration-dependent manner (Fig. 6f).

3.4.3. Effects of AOFOS on oxalic acid-induced precipitation and supernatant cellular injury

According to the result shown in Section 3.3.3, it was speculated that AOFOS slowed down the rate of crystal formation and increased the time for free oxalate ions to act on cells, ultimately resulting in decreased cell viability. Another possible reason may be that AOFOS promoted the formation of smaller crystals (Fig. 6a, b, c), which were more likely the cause of increased cytotoxicity (Sun et al., 2015).

To verify our hypothesis, oxalic acid was first treated with the culture medium containing various concentrations of AOFOS for 3 h to produce precipitates, and then the cells were cultured separately with the obtained precipitation and supernatant. As indicated in Fig. 6g, compared to the blank control group and supernatant group, the supernatant had a damaging effect on cells ($p < 0.05$), which may be related to the lack of calcium ions in the medium (Fig. 6g). However, cell culture by precipitation showed no cytotoxicity (Fig. 6h). Based on the above cell experiments and literature, the following hypothesis can be drawn: (1) Oxalate exposure induces a disruption of phosphatidylserine (PS) distribution in the renal epithelial cell membranes, and PS externalized into the exoplasmic leaflet serves as an attachment site, thereby promoting the retention of calcium oxalate monohydrate (COM) crystals at the cell surface (Bigelow et al., 1997; Cao et al., 2001; Khan, 2006). Cell damage mainly came from the action of oxalate ions in a short period of time, and the formation of calcium oxalate crystals was beneficial for reducing cell damage as oxalate passes through the urinary system compared with precipitation and oxalic acid groups. (2) The formation rate of calcium oxalate crystal was very fast. Although the cytotoxic activity was increased with AOFOS intervention (Fig. 6f) in the short term, the formation of large crystals was inhibited in the long term, which would increase the possibility of small crystal excretion in the urinary system reducing urinary tract blockage by stones.

4. Conclusions

In this study, AOFOS that could inhibit the formation of calcium oxalate crystals was purified and structurally characterized by MS, NMR and GPC. AOFOS significantly reduced the size of calcium oxalate crystals in Drosophila by inhibiting the formation of large size crystals and the generation rate of calcium oxalate crystals, as well as the COM crystallization. AOFOS is expected to exert a desirable effect in the prevention and treatment of urolithiasis.

CRediT authorship contribution statement

Peng Sun: Methodology, Data curation, Investigation, Software, Writing – original draft. **Shang-Gao Liao:** Writing – review & editing. **Rao-Qiong Yang:** Data curation, Investigation, Software. **Chuan-Li Lu:** Writing – review & editing. **Kai-Long Ji:** Writing – review & editing. **Dong-Hua Cao:** Writing – review & editing. **Hua-Bin Hu:** Resources. **Jian-Mei Lu:** Writing – review & editing. **Xing-Zhen Song:** Investigation. **Min Wu:** Investigation. **Hui-Zhen Jia:** Investigation. **Chun-Fen Xiao:** Resources. **Zhi-Wei Ma:** Investigation. **You-Kai Xu:** Conceptualization, Funding acquisition, Project administration, Methodology, Supervision.

Declaration of competing interest

The authors declare that they have no known competing financial interests or personal relationships that could have appeared to influence the work reported in this paper.

Acknowledgments

This work was supported by One Belt and One Road Ethnic Medicine Research and Industry Cooperation of the Cooperation Bureau of Chinese Academy of Sciences (Y6ZK131B01). Special thanks are given to the Central Laboratory of XTBG for the technical support of this study.

Appendix A. Supplementary data

Supplementary data to this article can be found online at https://doi.org/10.1016/j.carbpol.2022.119777.

References

Aggarwal, K. P., Narula, S., Kakkar, M., & Tandon, C. (2013). Nephrolithiasis: Molecular mechanism of renal stone formation and the critical role played by modulators. *BioMed Research International, 2013*, Article 292953. https://doi.org/10.1155/2013/292953

Akin, B., Öner, M., Bayram, Y., & Demadis, K. D. (2008). Effects of carboxylate-modified, "green" inulin biopolymers on the crystal growth of calcium oxalate. *Crystal Growth and Design, 8*, 1997–2005. https://doi.org/10.1021/cg800092q

Ali, S. N., Dayarathna, T. K., Ali, A. N., Osumah, T., Ahmed, M., Cooper, T. T., … Leong, H. S. (2018). Drosophila melanogaster as a function-based high-throughput screening model for anti-nephrolithiasis agents in kidney stone patients. *Disease Models & Mechanisms, 11*(11), Article dmm035873. https://doi.org/10.1242/dmm.035873

Ansari, M. S., Gupta, N. P., Hemal, A. K., Dogra, P. N., Seth, A., Aron, M., & Singh, T. P. (2005). Spectrum of stone composition: Structural analysis of 1050 upper urinary tract calculi from northern India. *International Journal of Urology, 12*, 12–16. https://doi.org/10.1111/j.1442-2042.2004.00990.x

Asselman, M., Verhulst, A., Van Ballegooijen, E. S., Bangma, C. H., Verkoelen, C. F., & De Broe, M. E. (2005). Hyaluronan is apically secreted and expressed by proliferating or regenerating renal tubular cells. *Kidney International, 68*, 71–83. https://doi.org/10.1111/j.1523-1755.2005.00382.x

Bigelow, M. W., Wiessner, J. H., Kleinman, J. G., & Mandel, N. S. (1997). Surface exposure of phosphatidylserine increases calcium oxalate crystal attachment to IMCD cells. *American Journal of Physiology-Renal Physiology, 272*, F55–F62. https://doi.org/10.1152/ajprenal.1997.272.1.F55

Cao, L. C., Jonassen, J., Honeyman, T. W., & Scheid, C. (2001). Oxalate-induced redistribution of phosphatidylserine in renal epithelial cells. *American Journal of Nephrology, 21*, 69–77. https://doi.org/10.1159/000046224

Chen, Y. H., Liu, H. P., Chen, H. Y., Tsai, F. J., Chang, C. H., Lee, Y. J., Lin, W. Y., & Chen, W. C. (2011). Ethylene glycol induces calcium oxalate crystal deposition in malpighian tubules: A drosophila model for nephrolithiasis/urolithiasis. *Kidney International, 80*, 369–377. https://doi.org/10.1038/ki.2011.80

Chen, Y. K., Lin, H. C., Chen, C. S., & Yeh, S. D. (2008). Seasonal variations in urinary calculi attacks and their association with climate: A population based study. *Journal of Urology, 179*, 564–569. https://doi.org/10.1016/j.juro.2007.09.067

Daudon, M., Bazin, D., & Letavernier, E. (2014). Randall's plaque as the origin of calcium oxalate kidney stones. *Urolithiasis, 43*, 5–11. https://doi.org/10.1007/s00240-014-0703-y

De Oliveira, A. J. B., Gonçalves, R. A. C., Chierrito, T. P. C., Dos Santos, M. M., De Souza, L. M., Gorin, P. A. J., Sassaki, G. L., & Iacomini, M. (2011). Structure and degree of polymerisation of fructooligosaccharides present in roots and leaves of Stevia rebaudiana (Bert.) bertoni. *Food Chemistry, 129*, 305–311. https://doi.org/10.1016/j.foodchem.2011.04.057

Dominique, S., Oscar, C., & Chiara, R. (2008). Gas chromatographic/mass spectrometric analysis of on-line pyrolysis–silylation products of monosaccharides. *Journal of Analytical and Applied Pyrolysis, 83*, 157–164. https://doi.org/10.1016/j.jaap.2008.07.006

Gan, Q. Z., Sun, X. Y., Bhadja, P., Yao, X. Q., & Ouyang, J. M. (2016). Reinjury risk of nano-calcium oxalate monohydrate and calcium oxalate dihydrate crystals on injured renal epithelial cells: Aggravation of crystal adhesion and aggregation. *International Journal of Nanomedicine, 11*, 2839–2854. https://doi.org/10.2147/IJN.S104505

Grohe, B., O'Young, J., Ionescu, D. A., Lajoie, G., Rogers, K. A., Karttunen, M., Goldberg, H. A., & Hunter, G. K. (2007). Control of calcium oxalate crystal growth by face-specific adsorption of an osteopontin phosphopeptide. *Journal of the American Chemical Society, 129*, 14946–14951. https://doi.org/10.1021/ja0745613

Han, Y. W., & Clarke, M. A. (1990). Production and characterization of microbial Levan. *Journal of Agricultural and Food Chemistry, 38*, 393–396. https://doi.org/10.1021/jf00092a011

Hu, M. G., Li, Y. H., Sun, Z. C., Huo, X. W., Zhu, N. L, Sun, Z. G., … Li, G. (2018). New polyoxypregnane glycosides from aspidopterys obcordata vines with antitumor activity. *Fitoterapia, 129*, 203–209. https://doi.org/10.1016/j.fitote.2018.07.003

Khan, A., Bashir, S., & Khan, S. R. (2021). Antiurolithic effects of medicinal plants: Results of in vivo studies in rat models of calcium oxalate nephrolithiasis—A systematic review. *Urolithiasis, 49*, 95–122. https://doi.org/10.1007/s00240-020-01236-0

Khan, S. R. (2006). Renal tubular damage/dysfunction: Key to the formation of kidney stones. *Urological Research, 34*, 86–91. https://doi.org/10.1007/s00240-005-0016-2

Li, F., Wei, Y., Liang, L., Huang, L., Yu, G., & Li, Q. (2021). A novel low-molecular-mass pumpkin polysaccharide: Structural characterization, antioxidant activity, and hypoglycemic potential. *Carbohydrate Polymers, 251*, Article 117090. https://doi.org/10.1016/j.carbpol.2020.117090

Li, J. K., Zhang, X., Cao, L. Y., Ji, J. J., & Gao, J. P. (2018). Three inulin-type fructans from Codonopsis pilosula (Franch.) nannf. Roots and their prebiotic activity on bifidobacterium longum. *Molecules, 23*(12), 3123. https://doi.org/10.3390/molecules23123123

Li, Y. H., Ma, G. X., Lv, Y. N., Su, J., Li, G., & Chen, X. (2019). Efficacy of obcordata a from aspidopterys obcordata on kidney stones by inhibiting NOX4 expression. *Molecules, 24*(10), 1957. https://doi.org/10.3390/molecules24101957

Li, Y. H., Li, G., Song, M. F., Li, X. L., Zhan, X., Lu, J., & Chen, X. (2016). Acute toxicity study of aspidopterys obcordata aqueous extract in Sprague-dawley rats. *Journal of Traditional Chinese Medicine, 36*, 377–381. https://doi.org/10.1016/S0254-6272(16)30052-8

Li, Y. F., Yu, S. L., Gan, X. G., Zhang, Z., Wang, Y., Wang, Y. W., & An, R. H. (2017). MRP-1 and BCRP promote the externalization of phosphatidylserine in oxalate-treated renal epithelial cells: Implications for calcium oxalate urolithiasis. *Urology, 107*, 271.e9–271.e17. https://doi.org/10.1016/j.urology.2017.05.034

Lin, Y. F., Yi, Z., & Zhao, Y. H. (2003). *Chinese Dai Medicine Colorful Illustrations* (pp. 540–541).

Liu, H., Sun, X. Y., Wang, F. X., & Ouyang, J. M. (2020). Regulation on calcium oxalate crystallization and protection on HK-2 cells of tea polysaccharides with different molecular weights. *Oxidative Medicine and Cellular Longevity, 2020*, Article 5057123. https://doi.org/10.1155/2020/5057123

Lotan, Y., Buendia Jiménez, I., Lenoir-Wijnkoop, I., Daudon, M., Molinier, L., Tack, I., & Nuijten, M. J. C. (2013). Increased water intake as a prevention strategy for recurrent urolithiasis: Major impact of compliance on cost-effectiveness. *Journal of Urology, 189*, 935–939. https://doi.org/10.1016/j.juro.2012.08.254

Maurice-Estepa, L., Levillain, P., Lacour, B., & Daudon, M. (2000). Advantage of zero-crossing-point first-derivative spectrophotometry for the quantification of calcium oxalate crystalline phases by infrared spectrophotometry. *Clinica Chimica Acta, 298*, 1–11. https://doi.org/10.1016/S0009-8981(00)00224-2

Mensink, M. A., Frijlink, H. W., Van Der Voort Maarschalk, K., & Hinrichs, W. L. J. (2015). Inulin, a flexible oligosaccharide I: Review of its physicochemical characteristics. *Carbohydrate Polymers, 130*, 405–419. https://doi.org/10.1016/j.carbpol.2015.05.026

Peng, Q. L., Li, C. Y., Zhao, Y. W., Sun, X. Y., Liu, H., & Ouyang, J. M. (2021). Protective effect of degraded porphyra yezoensis polysaccharides on the oxidative damage of renal epithelial cells and on the adhesion and endocytosis of nanocalcium oxalate crystals. *Oxidative Medicine and Cellular Longevity, 2021*, 1–15. https://doi.org/10.1155/2021/6463281

Penniston, K. L., McLaren, I. D., Greenlee, R. T., & Nakada, S. Y. (2011). Urolithiasis in a rural Wisconsin population from 1992 to 2008: Narrowing of the male-to-female ratio. *Journal of Urology, 185*, 1731–1736. https://doi.org/10.1016/j.juro.2010.12.034

R Core Team. (2020). *R: a language and environment for statistical computing*. Vienna, Austria: R Foundation for Statistical Computing. https://www.R-project.org/.

Roberfroid, M. B. (2005). Introducing inulin-type fructans. *British Journal of Nutrition, 93*, S13–S25. https://doi.org/10.1079/bjn20041350

Semangoen, T., Sinchaikul, S., Chen, S. T., & Thongboonkerd, V. (2008). Altered proteins in MDCK renal tubular cells in response to calcium oxalate dihydrate crystal adhesion: A proteomics approach. *Journal of Proteome Research, 7*, 2889–2896. https://doi.org/10.1021/pr800113k

Song, M. F., Li, Y. H., Zhang, Z. L., Lv, Y. N., Li, X. L., & Li, G. (2015). Inhibiting effect of Aspidopterys obcordata Hemsl. on renal calculus. *Chinese Journal New Drugs, 24*(9), 1047–1052.

Sorokin, I., Mamoulakis, C., Miyazawa, K., Rodgers, A., Talati, J., & Lotan, Y. (2017). Epidemiology of stone disease across the world. *World Journal of Urology, 35*, 1301–1320. https://doi.org/10.1007/s00345-017-2008-6

Spernat, D., & Kourambas, J. (2011). Urolithiasis - medical therapies. *BJU International, 108*, 9–13. https://doi.org/10.1111/j.1464-410X.2011.10688.x

Sun, P., Cao, D. H., Xiao, Y. D., Zhang, Z. Y., Wang, J. N., Shi, X. C., Xiao, C. F., Hu, H. B., & Xu, Y. K. (2020). Aspidoptoids A-D: Four new diterpenoids from aspidopterys obcordata vine. *Molecules, 25*(3), 529. https://doi.org/10.3390/molecules25030529

Sun, X. Y., Ouyang, J. M., Liu, A. J., Ding, Y. M., & Gan, Q. Z. (2015). Preparation, characterization, and in vitro cytotoxicity of COM and COD crystals with various sizes. *Materials Science and Engineering C, 57*, 147–156. https://doi.org/10.1016/j.msec.2015.07.032

Sun, X. Y., Zhang, H., Chen, J. Y., Zeng, G. H., & Ouyang, J. M. (2021). Porphyra yezoensis polysaccharide and potassium citrate synergistically inhibit calcium oxalate crystallization induced by renal epithelial cells and cytotoxicity of the formed crystals. *Materials Science and Engineering C, 119*, Article 111448. https://doi.org/10.1016/j.msec.2020.111448

Taylor, E. N., Stampfer, M. J., & Curhan, G. C. (2010). The risk of kidney stones. *JAMA, 293*, 455–462. https://www.ncbi.nlm.nih.gov/pubmed/15671430.

Trinchieri, A., Castelnuovo, C., Lizzano, R., & Zanetti, G. (2005). Calcium stone disease: A multiform reality. *Urological Research, 33*, 194–198. https://doi.org/10.1007/s00240-004-0459-x

Türk, C., Petřík, A., Sarica, K., Seitz, C., Skolarikos, A., Straub, M., & Knoll, T. (2016). EAU guidelines on interventional treatment for urolithiasis. *European Urology, 69*, 475–482. https://doi.org/10.1016/j.eururo.2015.07.041

Yao, X. Q., Ouyang, J. M., Peng, H., Zhu, W. Y., & Chen, H. Q. (2012). Inhibition on calcium oxalate crystallization and repair on injured renal epithelial cells of degraded soybean polysaccharide. *Carbohydrate Polymers, 90*, 392–398. https://doi.org/10.1016/j.carbpol.2012.05.056

Yasui, T., Fujita, K., Tozawa, K., Asai, K., Soji, T., Kato, T., & Kohri, K. (2001). Calcium oxalate crystal attachment to cultured rat kidney epithelial cell, NRK-52E. *Urologia Internationalis, 67*, 73–76. https://doi.org/10.1159/000050949

Zhang, H., Sun, X. Y., Chen, X. W., & Ouyang, J. M. (2020). Degraded: Porphyra yezoensis polysaccharide protects HK-2 cells and reduces nano-COM crystal toxicity, adhesion and endocytosis. *Journal of Materials Chemistry B, 8*, 7233–7252. https://doi.org/10.1039/d0tb00360c

Zhang, S. J., Song, Z. T., Shi, L. J., Zhou, L. N., Zhang, J., Cui, J. L., … Guo, Y. Q. (2021). A dandelion polysaccharide and its selenium nanoparticles: Structure features and evaluation of anti-tumor activity in zebrafish models. *Carbohydrate Polymers, 270*, Article 118365. https://doi.org/10.1016/j.carbpol.2021.118365

Zhang, X., Hu, P., Zhang, X. R., & Li, X. J. (2020). Chemical structure elucidation of an inulin-type fructan isolated from Lobelia chinensis Lour with anti-obesity activity on diet-induced mice. *Carbohydrate Polymers, 240*, Article 116357. https://doi.org/10.1016/j.carbpol.2020.116357